Circuit-specific control of the medial entorhinal inputs to the dentate gyrus by atypical presynaptic NMDARs activated by astrocytes

Iaroslav Savtchouk[a,1], Maria Amalia Di Castro[a,1], Rugina Ali[a,1], Hiltrud Stubbe[a], Rafael Luján[b], and Andrea Volterra[a,2]

[a]Département de Neurosciences Fondamentales, Université de Lausanne, 1005 Lausanne, Switzerland; and [b]Synaptic Structure Laboratory, Instituto de Investigación en Discapacidades Neurológicas, Departamento Ciencias Médicas, Facultad de Medicina, Universidad Castilla-La Mancha, 02071 Albacete, Spain

Edited by Per Jesper Sjöström, McGill University, Montreal, Canada, and accepted by Editorial Board Member Gina G. Turrigiano May 5, 2019 (received for review September 18, 2018)

Here, we investigated the properties of presynaptic *N*-methyl-D-aspartate receptors (pre-NMDARs) at corticohippocampal excitatory connections between perforant path (PP) afferents and dentate granule cells (GCs), a circuit involved in memory encoding and centrally affected in Alzheimer's disease and temporal lobe epilepsy. These receptors were previously reported to increase PP release probability in response to gliotransmitters released from astrocytes. Their activation occurred even under conditions of elevated Mg^{2+} and lack of action potential firing in the axons, although how this could be accomplished was unclear. We now report that these pre-NMDARs contain the GluN3a subunit conferring them low Mg^{2+} sensitivity. GluN3a-containing NMDARs at PP-GC synapses are preponderantly presynaptic vs. postsynaptic and persist beyond the developmental period. Moreover, they are expressed selectively at medial—not lateral—PP axons and act to functionally enhance release probability specifically of the medial perforant path (MPP) input to GC dendrites. By controlling release probability, GluN3a-containing pre-NMDARs also control the dynamic range for long-term potentiation (LTP) at MPP-GC synapses, an effect requiring Ca^{2+} signaling in astrocytes. Consistent with the functional observations, GluN3a subunits in MPP terminals are localized at sites away from the presynaptic release sites, often facing astrocytes, in line with a primary role for astrocytic inputs in their activation. Overall, GluN3A-containing pre-NMDARs emerge as atypical modulators of dendritic computations in the MPP-GC memory circuit.

presynaptic | NMDAR | GluN3a | plasticity | astrocyte

Excitatory projections from the entorhinal cortex (EC) to the dentate gyrus (DG) play a central role in memory encoding (1) and are also severely impacted in humans affected by Alzheimer's disease (AD) and temporal lobe epilepsy (TLE) (2), critically contributing to the dysfunctions typical of these pathologies (3, 4). All EC projections to DG make glutamatergic synapses onto dentate granule cells (GCs) but with different functional properties depending on the afferents coming from the lateral perforant path (LPP) or medial perforant path (MPP). MPP synapses show higher presynaptic release probability than LPP synapses (5). Another difference is in the susceptibility to pathology, with LPP (but not MPP) synapses showing release probability changes in epilepsy models (6), preferential amyloid-β deposition (7), earlier susceptibility in AD (8), and reduced plasticity with age (9). The reasons for such differences are unknown.

We and others have previously shown that perforant path (PP) projections onto dentate GCs are modulated by astrocytes not only through high expression of membrane glutamate transporters but also, via gliotransmitter release onto ifenprodil-sensitive presynaptic *N*-methyl-D-aspartate (NMDA) receptors (pre-NMDARs) (10). Visualized by electron microscopy (EM), GluN2b-containing pre-NMDARs are typically located in PP terminals away from the synaptic cleft, directly facing astrocytic membranes (10, 11). The presence of direct astrocyte–PP axon contacts is supported by rabies virus tracing studies (12). Rabies virus retrogradely labels presynaptic cells: in this case, it traveled from the infected PP projections to a portion of DG astrocytes, consistent with the existence of dedicated astrocyte-to-axon release sites with specialized release machinery (10, 11).

Dynamic modulation of PP release can be elicited by astrocyte stimulation (e.g., via direct depolarization or on activation of astrocytic purinergic G protein-coupled receptor P2Y1). Consistently, inhibition of astrocytic signaling by blocking P2Y1 receptors, internal Ca^{2+} elevation, or exocytosis eliminates the astrocyte modulation (10, 13–15). Moreover, astrocyte signaling via type 1 tumor necrosis factor-α receptors (TNFR1s), activated by pathological levels of the cytokine, changes PP release probability persistently (14). Surprisingly, all of these presynaptic effects of astrocytes were observed in the presence of 2 mM extracellular Mg^{2+}, suggesting that pre-NMDARs in DG have low Mg^{2+} sensitivity, despite containing GluN2b subunits.

NMDARs have been implicated both in physiological processes, such as memory formation, and in pathological ones, such as those underlying drug addiction, AD, schizophrenia, or stroke

Significance

We previously identified a mechanism controlling transmitter release probability at perforant path (PP)–granule cell excitatory synapses, a memory-related circuit that goes awry in Alzheimer's disease and temporal lobe epilepsy. We found that the mechanism involves activation of presynaptic *N*-methyl-D-aspartate receptors (pre-NMDARs) by astrocytes but could not explain its specificities, notably why pre-NMDARs were activated in conditions in which classical NMDARs are not. We show that pre-NMDARs (*i*) contain an atypical subunit, GluN3a, responsible for their properties and (*ii*) are localized in PP terminals facing astrocytes, restricted to a subset of PP afferents and controlling only the synapses made by those afferents. This circuit-specific modulatory mechanism by astrocytes may be important for memory processing and its alterations in pathological conditions.

Author contributions: I.S. and A.V. designed research; I.S., M.A.D.C., R.A., H.S., and R.L. performed research; I.S., M.A.D.C., R.A., and R.L. analyzed data; H.S. characterized and maintained GluN3a$^{-/-}$ colonies and related littermate controls; R.L. designed electron microscopy experiments; and I.S., M.A.D.C., and A.V. wrote the paper.

The authors declare no conflict of interest.

This article is a PNAS Direct Submission. P.J.S. is a guest editor invited by the Editorial Board.

[1]I.S., M.A.D.C., and R.A. contributed equally to this work.

[2]To whom correspondence may be addressed. Email: andrea.volterra@unil.ch.

This article contains supporting information online at www.pnas.org/lookup/suppl/doi:10.1073/pnas.1816013116/-/DCSupplemental.

(reviewed in refs. 16 and 17). While a majority of these processes involve NMDARs located on the postsynaptic membrane, presynaptic localization of NMDARs permits a unique way to modulate synaptic strength by changing release probability and thus, efficacy of synaptic transmission. In the hippocampal PP, a single presynaptic varicosity is contacted by multiple postsynaptic spines (18, 19), allowing a presynaptic change at a single bouton to simultaneously modulate the strength at multiple postsynapses. In addition to our observations (10, 11), other studies reported data consistent with the presence of pre-NMDAR at PP-GC synapses, notably ifenprodil-sensitive ones (20). Moreover, NMDARs with presynaptic location have been increasingly reported and functionally investigated in several brain regions, including cerebellum, cortex, and hippocampus (21–35). However, there have also been reports challenging the above observations (36, 37) and raising debate about the existence of pre-NMDAR (38). One pervasive difficulty in prior studies was distinguishing true pre-NMDAR activation from unintentional somatodendritic NMDAR activation in a presynaptic cell, which could then spread to the axon (37). In this respect, hippocampal PP provides an ideal system to isolate somatic and axonal components, because PP axons can span over a millimeter between source EC pyramidal cells and target GC in the hippocampus.

Pre-NMDAR expression seems to vary both with the circuits studied and with age (34, 39–43). Subunit composition also has a large effect on receptor function. Structurally, NMDARs are tetramers that can be composed of two GluN1 subunits and two GluN2 and/or GluN3 subunits. The exact subunit composition will determine the kinetics of the NMDAR channel, its Mg^{2+} sensitivity, and Ca^{2+} permeability (reviewed in ref. 44). Incorporation of GluN2c, GluN2d (45), or GluN3 subunits drastically lowers Ca^{2+} permeability and voltage-dependent Mg^{2+} block (reviewed in refs. 16 and 46), allowing, in some instances, receptor opening even at resting membrane potential (47, 48). This property is shared by NMDARs found to use unconventional metabotropic signaling via conformational changes without ion flux through the channel (49, 50).

Some of the receptor subunits are developmentally regulated. For example, GluN3a reaches peak whole-brain expression at ~P8 and gradually decreases with maturation (34, 51, 52). However, at certain afferents, GluN3 expression was reported to persist well into adulthood (reviewed in ref. 46).

Since pre-NMDARs at PP-GC synapses have low Mg^{2+} sensitivity, we tested whether metabotropic signaling or incorporation of subunits, like GluN3a, accounted for their specific properties.

Results

Transient Local NMDA Application Increases Release Probability at PP-GC Synapses. GluN2b-containing pre-NMDARs on PP axon terminals respond to targeted gliotransmitter release from astrocytes by increasing release probability of PP-GC synapses (10). To better examine the role and properties of these pre-NMDARs, we now stimulated them via brief local puff applications of exogenous NMDA (5 μM) while monitoring α-amino-3-hydroxy-5-methyl-4-isoxazolepropionic acid receptor (AMPAR)-mediated miniature excitatory postsynaptic currents (mEPSCs) in patched GCs. We used experimental conditions apt at minimizing activation of NMDARs in GCs (10), including 2 mM Mg^{2+} and tetrodotoxin (TTX) in the bathing medium, the high-affinity NMDAR blocker (MK-801; 1 mM) in the patch pipette, and hyperpolarization of the patched GC at −80 mV (Fig. 1*A*). Dependably, our NMDA puffs increased mEPSC frequency (Fig. 1 *B* and *C*) without

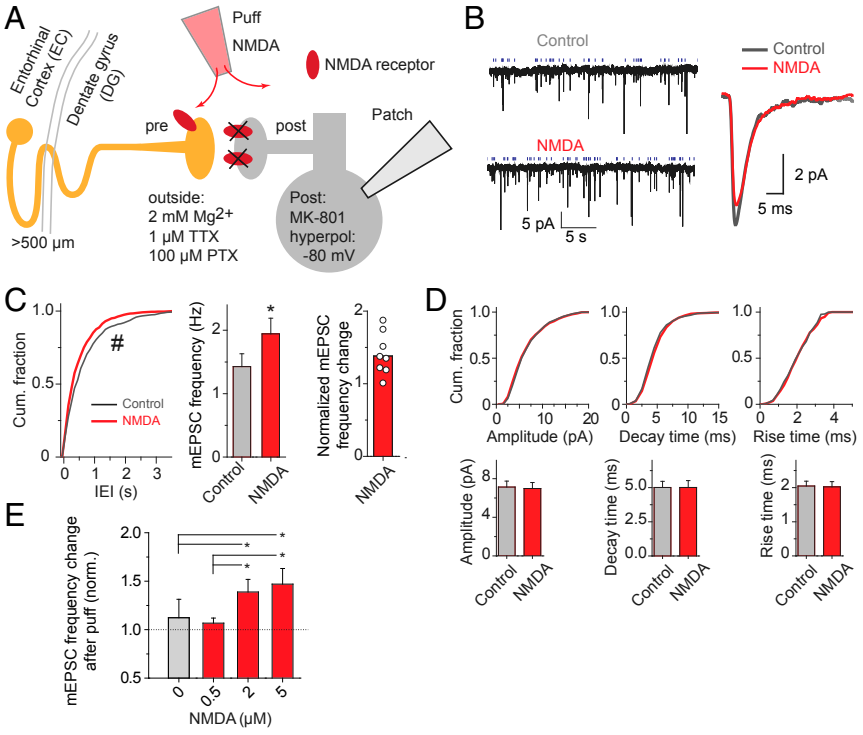

Fig. 1. Puff application of NMDA increases release probability at PP-GC synapses of juvenile mice. (*A*) Schematic drawing of the experimental approach. mEPSCs were recorded from a patched GC before and after focal NMDA puff application (14) in artificial cerebrospinal fluid (aCSF) containing 2 mM Mg^{2+}, TTX, and picrotoxin (PTX). Activation of GC NMDARs was minimized by hyperpolarizing the cell and dialyzing it with intracellular MK-801 (10). (*B*) Example synaptic current traces showing increased mEPSC frequency after 5 μM NMDA puff. Detected events are indicated by tick marks above traces. (*C*) Group data showing decreased interevent interval (IEI; KS test, $n = 453$ vs. 473 events) and increased mEPSC frequency on NMDA puff. Significance: *paired t test $P < 0.05$; $^{\#}P < 0.05$. (*D*) mEPSC amplitude and kinetics were not affected by NMDA. (*E*) Puff-induced increase in mEPSC frequency was achieved at NMDA concentrations ≥2 μM (Kruskal–Wallis test, $P = 0.025$; multiple comparisons at 95% confidence value, $n = 5$–8 each, $^{*}P < 0.05$).

changing events' amplitude and kinetics (Fig. 1*D*), consistent with a presynaptic effect. To exclude artifacts of the puff application (e.g., mechanic stimulation of nearby astrocytes), we performed identical puffs into the tissue without NMDA [artificial CSF (aCSF) solution] and observed no potentiation. Likewise, NMDA applied at 0.5 μM was ineffective, whereas at 2 μM, it increased mEPSC frequency (Fig. 1*E*), suggesting a low micromolar threshold for its action at pre-NMDARs.

Pre-NMDARs Do Not Function as Autoreceptors for Tonic Control of Basal Glutamate Release. We then investigated whether pre-NMDARs at PP-GC synapses tonically regulate spontaneous glutamate release as reported at various cortical and hippocampal connections (22, 34, 45, 53). To this end, we bath applied the broad-spectrum NMDAR antagonist D-2-amino-5-phosphonovalerate (D-APV) (50 μM) and looked for mEPSC changes (Fig. 2*A*). In fact, no change was observed in mEPSC frequency (Fig. 2*B*), amplitude, or kinetics (Fig. 2*C*). Therefore, pre-NMDARs at PP-GC synapses do not function as autoreceptors involved in modulating the basal release probability.

Activity-Dependent Pre-NMDARs Stimulation Changes Release Probability at MPP but Not LPP Synapses. To investigate whether pre-NMDARs at PP-GC synapses are activated by evoked glutamate release, we performed paired pulse stimulations of PP fibers and recorded evoked EPSCs (eEPSCs) in GCs. We stimulated MPP and LPP afferents separately and compared the effect of pre-NMDARs at the two distinct inputs on GCs. Because pre-NMDARs at PP terminals contain GluN2b (10) and because GluN2b-containing NMDARs at PP-GC synapses are preponderantly presynaptic (10, 13, 15, 20), we used for these experiments the GluN2b-selective antagonist ifenprodil (3 μM). Application of the drug caused combined decrease in eEPSC amplitude and increase in evoked paired pulse ratio (PPR), generally interpretable as a pure presynaptic effect (Fig. 2 *D* and *E*). However and surprisingly, this effect was restricted to MPP synapses, whereas ifenprodil produced no effect at LPP synapses (Fig. 2 *D* and *E*). To exclude that this depended on a larger readily releasable pool (RRP) or on an action of pre-NMDARs at LPP synapses on RRP replenishment rate rather than on release probability, we applied a long train of pulses (30 Hz) sufficient to deplete the RRP (54) (*SI Appendix*, Fig. S1). However, ifenprodil was still devoid of any effect, while lowering external Ca^{2+} (1 mM), which reduces RRP size, produced the expected functional changes (54). Therefore, modulation of release probability by GluN2b-containing pre-NMDAR is a circuit-specific feature of MPP-GC synapses.

Removal of GluN3a Subunit Abolishes Pre-NMDAR–Dependent Modulation of MPP Synapses but Has No Effect at LPP Synapses. The effect of NMDA on mEPSCs at MPP-GC synapses is puzzling considering that ifenprodil-sensitive GluN2b confers to NMDAR high Mg^{2+} sensitivity requiring depolarization-dependent channel unblocking, while NMDA increased mEPSC frequency (Fig. 1) in the presence of 2 mM extracellular Mg^{2+}. This result could be explained if pre-NMDARs acted metabotropically (49, 50) or contained additional subunits, such as GluN2c, GluN2d (45), or GluN3a, which reduce Mg^{2+} sensitivity (16). The first hypothesis was discarded, because 7-chlorokinurenic acid (100 μM), a drug that abolishes NMDAR ion flux but does not affect the receptor's metabotropic signaling (49), fully reproduced the effects of

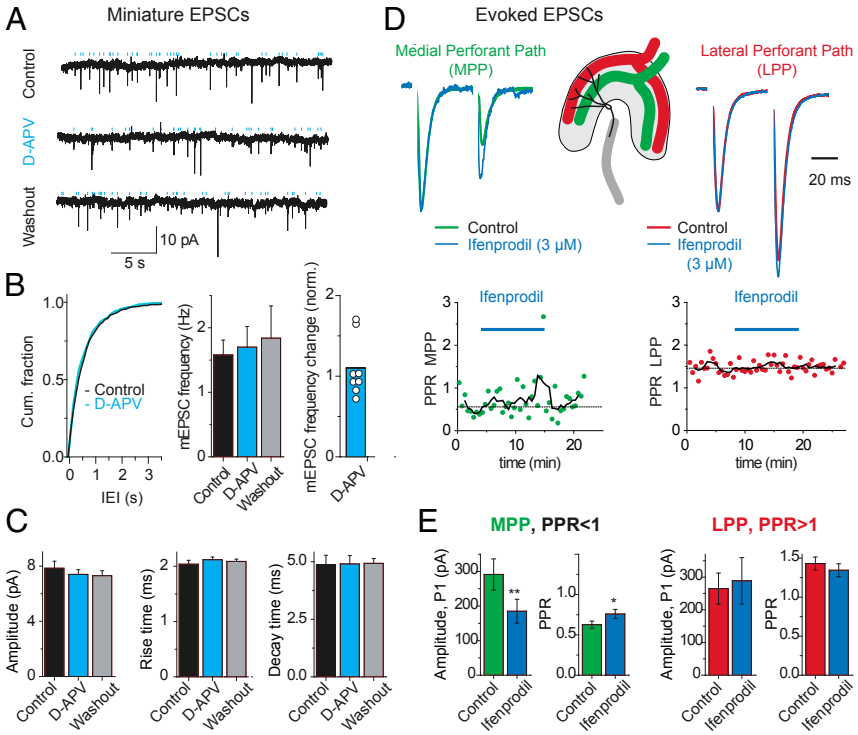

Fig. 2. Pre-NMDARs at PP-GC synapses lack activation under basal conditions but are recruited by electrical stimulation of MPP (but not LPP) afferents. (*A*) Example traces in a GC showing no changes in mEPSC frequency after bath application of the broad-spectrum NMDAR antagonist D-APV and its washout. (*B*) Group data showing that mEPSC frequency and interevent interval (IEI) were unaffected on D-APV application and subsequent washout (KS and paired *t* tests). (*C*) Likewise, mEPSC amplitude and kinetics were not affected by D-APV. (*D*, *Upper*) Representative paired pulse eEPSC responses in a GC in response to MPP (green) or LPP (red) stimulation in control condition and on application of 3 μM ifenprodil (blue). (*D*, *Lower*) Representative time course of ifenprodil effect on PPR at depressing MPP (PPR < 1) and facilitating LPP (PPR > 1) synapses (black lines are five-point running averages). (*E*) Ifenprodil application caused significant decrease in pulse 1 amplitude and increase in PPR at MPP but not LPP synapses (paired *t* test). $*P < 0.05$; $**P < 0.01$.

ifenprodil on eEPSC amplitude and PPR (*SI Appendix*, Fig. S2). To start addressing the second hypothesis, we exploited availability of GluN3a knockout mice in the laboratory (GluN3a$^{-/-}$) (51). Contrary to what was observed in wild-type mice (Fig. 1), NMDA puff in the knockouts did not change mEPSC frequency (Fig. 3 *A* and *B*), amplitude, or kinetics (Fig. 3*C*), revealing a necessary role for the GluN3a subunit in the presynaptic action of the drug. GluN3a removal per se did not affect baseline function of unstimulated PP-GC synapses (GluN3a$^{-/-}$ vs. wild type: mEPSC frequency, 1.91 ± 0.36 vs. 1.41 ± 0.13 Hz, *t* tests: $P > 0.10$; amplitude, 7.42 ± 0.30 vs. 6.96 ± 0.41, $P > 0.38$; rise time, 2.23 ± 0.13 vs. 2.08 ± 0.06, $P > 0.19$; decay time, 5.52 ± 0.38 vs. 5.03 ± 0.24, $P > 0.25$; $n = 10$ vs. 22 cells, respectively).

We then tested evoked synaptic responses at both MPP-GC and LPP-GC synapses in GluN3a$^{-/-}$ mice. The input–output curve at either connection did not differ significantly from the curve in littermate controls (*SI Appendix*, Fig. S3), suggesting that GluN3a ablation per se does not alter basal synaptic strength. However, it induced a small but significant PPR increase (Fig. 3 *D*, *Left*) selectively at MPP-GC synapses, signaling a changed control of release probability in the absence of this subunit. Moreover, ifenprodil application in GluN3a$^{-/-}$ mice did not change PPR (Fig. 3 *E*, *Left*), at variance with its effect in wild-type mice (Fig. 2*E*), suggesting that GluN3a ablation and ifenprodil converge in affecting the same pre-NMDAR–dependent mechanism controlling release probability at MPP-GC synapses. Lack of GluN3a did not produce any effect on PPR at LPP-GC synapses (Fig. 3 *D*, *Right*), even with combined ifenprodil application (Fig. 3 *E*, *Right*), confirming absence of pre-NMDAR modulation at these synapses.

GluN3a at PP-GC Synapses Is Mainly Presynaptic, Is Concentrated at MPP Terminals, and Like Pre-NMDAR–Dependent Modulation, Persists After Development. Our electrophysiological results strongly suggest that GluN3a-containing pre-NMDARs are differentially expressed at MPP vs. LPP. To probe this, we used preembedding immunogold EM in DG slices of juvenile and young adult mice (Fig. 4*A*). For each age group, we chose a representative number of positive synapses and quantified the relative (pre vs. post) distribution of GluN3a gold puncta at each synapse. In keeping with functional data, puncta were found to be concentrated at MPP terminals and almost undetectable at LPP terminals (Fig. 4 *A*, *a* and *b* vs. Fig. 4 *A*, *c* and *d* and *B*). While a few GluN3a particles were observed postsynaptically, the large majority were in MPP terminals at extrasynaptic locations away from the cleft, often facing astrocytic membranes (Fig. 4 *A*, *a Inset* and *b*). GluN3a staining in MPP terminals decreased with age but was still clearly detected beyond development (Fig. 4 *A*, *e* and *f*): particles counted at P45 were ∼50% of those at P21 (Fig. 4*B*). Accordingly, ∼50% of the recorded GCs in young adult mice showed mEPSC response to NMDA (Fig. 4 *C*, *Left*) and ∼60% PPR response to ifenprodil (Fig. 4 *C*, *Right*).

Long-Term Potentiation at MPP-GC Synapses Is Similarly Enhanced in GluN3a$^{-/-}$ Mice and in Control Mice with Blocked Astrocyte Ca^{2+} Signaling. Since long-term potentiation (LTP) at MPP-GC synapses has been associated with presynaptic increase in glutamate release (5), we next investigated the impact of GluN3a ablation on synaptic plasticity in this circuit. LTP induced by high-frequency stimulation (HFS) was compared in GluN3a$^{-/-}$ and littermate controls. For these experiments, we used local field potential recordings (Fig. 5*A*). On HFS, GluN3a$^{-/-}$ mice displayed significantly larger LTP in the recorded fields than controls (Fig. 5*B*), revealing an increased dynamic range for potentiation of these synapses in the absence of GluN3a. We next asked whether astrocytes are involved in this effect based on previous evidence that astrocytes are recruited by PP axons firing and respond to it by starting intracellular Ca^{2+} signaling that results in changed release probability of PP-GC synapses (15). Taking advantage of previously established protocols (10, 15, 55), we used wild-type littermate mice and recorded field potential responses in fields containing an astrocyte whole cell patched with internal solution containing the Ca^{2+} chelator 1,2-Bis(2-aminophenoxy)ethane *N,N,N′,N′*-tetraacetic acid (BAPTA) (40 mM) (Fig. 5*A*). HFS-LTP

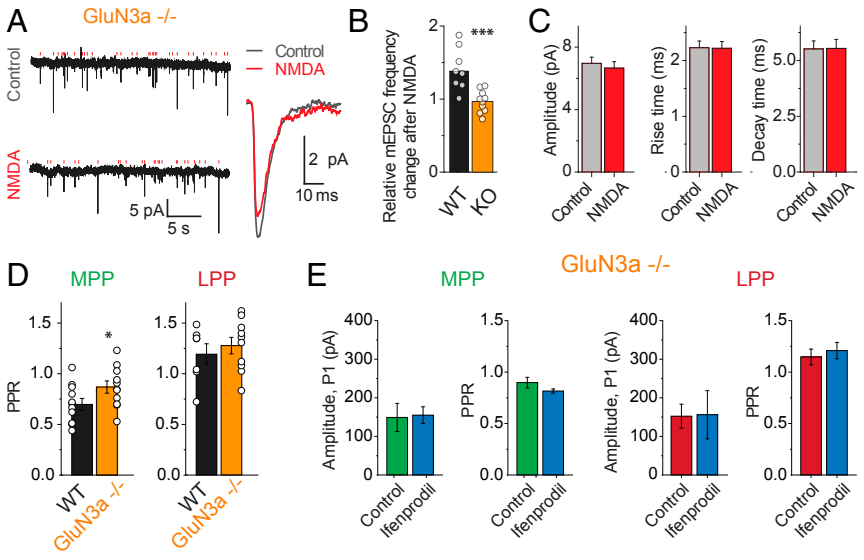

Fig. 3. GluN3a subunit is required for pre-NMDAR–dependent modulation of MPP but not LPP synapses. (*A*) Example traces and (*B*) group data showing that puff-applied NMDA (5 μM) does not trigger any mEPSC frequency increase in GluN3a$^{-/-}$ mice at variance with the effect in wild-type mice (*t* test).***$P < 0.005$ ($n = 10$ vs. 8). (*C*) Postsynaptic current parameters (amplitude, rise, and decay time) are not changed by NMDA application in GluN3a$^{-/-}$ mice. (*D*) Group data showing that PPRs of synaptic currents evoked by MPP stimulation (interstimulus interval = 50 ms) in GCs were larger in GluN3a$^{-/-}$ mice compared with wild-type littermates (Kruskal–Wallis; $n = 12$ vs. 11, *$P < 0.05$), while PPR measured on LPP stimulation were not significantly different between the two groups ($n = 10$ vs. 7). (*E*) In GluN3a$^{-/-}$ mice, ifenprodil application did not change eEPSC amplitude and PPR at both MPP and LPP synapses (paired *t* test: $n = 5$ both) at variance with its effect in wild-type mice (Fig. 2*E*, MPP). KO, knockout; WT, wild type.

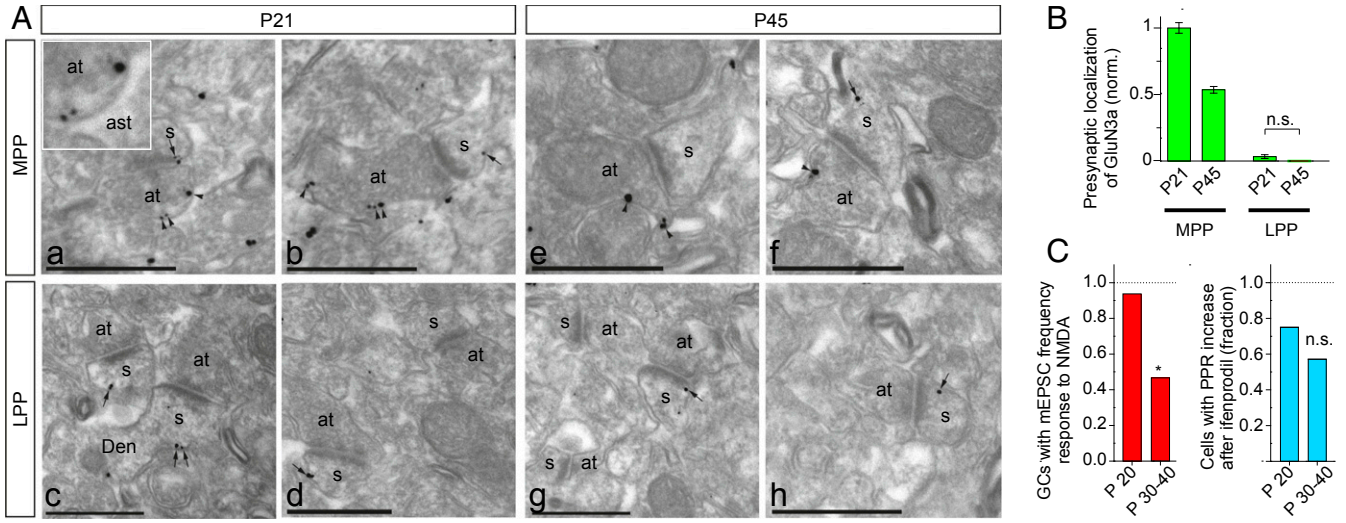

Fig. 4. GluN3a subunits are presynaptically expressed at MPP but not LPP axonal boutons in both juvenile and young adult mice. (*A*) Subcellular localization of GluN3a in the DG. Electron micrographs show immunoparticles for GluN3a as detected using the preembedding immunogold technique. At P21 (*A*, *a–d*), GluN3a immunoparticles in MPP (*A*, *a* and *b*) were preponderantly localized to the extrasynaptic plasma membrane (arrowheads) of axon terminals (at), establishing asymmetrical synapses with spines (s) on the dendrites (Den), often facing astrocytic profiles (ast; *A*, *a Inset*); with much lower frequency, they were also localized along the extrasynaptic plasma membrane (arrows) of dendritic spines. In contrast, LPP immunoparticles (*A*, *c* and *d*) were detected at low frequency and only along the extrasynaptic plasma membrane (arrows) of GC dendritic spines. At P45 (*E–H*), GluN3a immunoparticles in MPP (*A*, *e* and *f*) were still observed preponderantly along the extrasynaptic plasma membrane (arrowheads) of axon terminals compared with the extrasynaptic plasma membrane (arrows) of dendritic spines but at lower frequency than at P21. GluN3a immunoparticles in LPP (*A*, *g* and *h*) were detected at low frequency, lower than at P21, and only along the extrasynaptic plasma membrane (arrows) of GC dendritic spines. (Scale bars: 500 nm.) (*B*) Quantification of gold puncta relative distribution within GluN3a-positive axon terminals of MPP and LPP in P21 and P45 mice [for each condition: $n = 45$ GluN3a-positive synapses from three mice; one-way ANOVA on all four groups: $P < 0.05$, degrees of freedom = 3, F value = 365.67, Tukey post hoc: all pairwise comparisons significantly different at $P < 0.05$ except as indicated (n.s.)]. (*C*) GluN3a-dependent presynaptic modulation at MPP is observed both in juvenile (P20) and young adult (P30-40) mice. Pre-NMDARs continue to be observed electrophysiologically into adulthood as evidenced by persistence of effects of both NMDA application (*Left*; fraction of cells responding with increased mEPSC frequency in juvenile vs. young adult, $n = 16$ vs. 15, $P < 0.01$, χ^2 test: χ^2 statistic 8.3299, $^*P = 0.0039$) (Fig. 1) and ifenprodil application (*Right*; fraction of cells responding with eEPSC PPR change at MPP-GC synapses in juvenile vs. young adult, $n = 12$ vs. 7, $P = 0.4192$, χ^2 test: χ^2 statistic 0.6553) (Fig. 2).

measured in these fields was significantly larger than LTP measured, in separate experiments, in analogous fields in which astrocytes were not patched, astrocytes were patched without BAPTA, or a BAPTA-containing pipette was positioned proximal to the field electrode (Fig. 5*C*). Therefore, blockade of Ca^{2+} elevations in astrocytes reproduces the effect on LTP seen in GluN3a$^{-/-}$ mice, strongly suggesting that the two maneuvers interfere with the same mechanism and consequently, that recruitment of pre-NMDARs in LTP involves intermediary astrocyte signaling.

Discussion

Here, we investigated the properties of pre-NMDARs at corticohippocampal PP-GC synapses. Understanding such properties is important in view of the functional specificities of this circuit (e.g., in memory encoding) and of its malfunctioning in conditions, like multiple sclerosis, AD, and TLE. Previous work highlighted that pre-NMDARs in this circuit are peculiar, as they can activate paradoxically—despite containing the GluN2b subunit—even in 2 mM extracellular Mg^{2+} and TTX (10, 14). To explain such property, we explored unconventional modes of NMDAR function, such as metabotropic signaling (49), and eventually found that incorporation of a GluN3a subunit in the receptor can account for it. The time course of GluN3a expression and function at PP terminals is also atypical: while it classically peaks during early development (<P20) to drastically decrease with circuit maturation (46), here the subunit persists into early adulthood and possibly, longer (14). GluN3a immunoreactivity is still well detectable in MPP terminals at P45, and functional effects of Mg^{2+}-insensitive pre-NMDAR are present in a good portion of P30–P40 mice but are already wiped out in young mice lacking GluN3a.

Another intriguing property of GluN3a-containing pre-NMDARs at PP-GC synapses is their unavailability for tonic autoreceptor function in response to spontaneous glutamate release. Thus, a broad-spectrum NMDAR antagonist, D-APV, failed to affect mEPSCs frequency (Fig. 2 *A–C*), in stark contrast with its effectiveness in several other brain circuits expressing GluN3a-containing pre-NMDARs (22, 34, 45, 53). However, the effects of exogenous NMDA on mEPSCs and of NMDAR antagonists on eEPSCs and PPR indicate that pre-NMDARs activate under conditions of enhanced glutamate release. This could depend on spillover from neighboring synapses or on release from astrocytes or other cells. Synaptic spillover or mechanisms requiring glutamate diffusion at some distance seem unlikely given the high density of glutamate transporters in perisynaptic astrocytic processes (11) and the tight control that they exert on extracellular glutamate at these synapses (13), likely also preventing pre-NMDAR autoreceptor function. Release of glutamate from astrocytes seems, therefore, the most realistic, albeit unconventional, mechanism for pre-NMDARs activation at PP-GC synapses. Supporting convergent evidence includes that (*i*) astrocytes apparently form synaptic-like connections with PP axons and function as their "presynaptic" input (12); (*ii*) pre-NMDARs in MPP terminals are positioned mainly at sites facing astrocytes (10) (Fig. 4); (*iii*) astrocytic stimulation triggers Ca^{2+}-dependent glutamate release (10, 13), and moreover, it increases mEPSC frequency, like NMDA application, with both effects being ifenprodil sensitive (10, 13) (Fig. 1); and (*iv*) PP axonal firing recruits astrocyte Ca^{2+} signaling and suppression of this signaling depresses PP release probability (15, 56). Finally, even more direct support comes from these LTP experiments

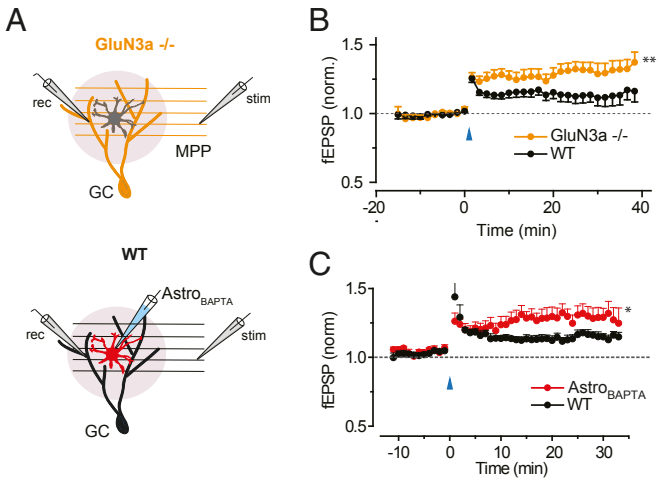

Fig. 5. The dynamic range for HFS-LTP at MPP-GC synapses increases in mice lacking GluN3a or on astrocyte-selective disruption of Ca^{2+} signaling in wild-type mice. (*A*) Schematic drawing of the LTP experiment (local field potential measures) in GluN3a$^{-/-}$ mice (*Upper*) or in wild-type animals with astrocytes whole-cell clamped using BAPTA-containing internal solution to block Ca^{2+} transients (*Lower*). (*B*) Tetanic HFS (100 Hz for 1 s, repeated three times) produces larger LTP in GluN3a$^{-/-}$ mice vs. wild-type mice (wild type: eight slices, GluN3a$^{-/-}$: seven slices). Statistics: KS tests on the (nonnormalized) values between 20 and 40 min postinduction: field excitatory postsynaptic potential (fEPSP) amplitude: KS statistics 0.266, PPR: KS statistic 0.2022. $^{**}P < 0.0001$. (*C*) Clamping astrocytic calcium (40 mM BAPTA) increases local LTP measured in close proximity of the patched astrocyte. $^{*}P < 0.001$. WT, wild type.

showing an identical effect on the plasticity by ablating GluN3a or perturbing Ca^{2+} signaling in astrocytes (Fig. 5).

GluN3a-containing NMDARs at PP-GC synapses are preponderantly presynaptic vs. postsynaptic. According to current understanding, presence of pre-NMDARs varies widely between different brain regions and circuits and may be tightly developmentally regulated (57, 58). Consistent with such diversity, we report a surprising specificity in pre-NMDAR localization in the DG: GluN3a-containing receptors are selectively expressed at MPP—not LPP—axons. Such segregation is robustly evident across several age cohorts (Fig. 4), electrophysiological paradigms (Figs. 2 and 3), and investigative techniques: EM and electrophysiology. It is presently unclear why there exists such a critical selectivity of MPP vs. LPP fibers in the capacity to modulate their inputs at nearby synapses onto the same GC. The case, however, is not unique. Similar differential modulation of two inputs converging onto the same target has been reported (e.g., in the cerebellum, where Purkinje cells receive functionally distinct excitatory inputs from PPR-depressing climbing fibers and from strongly PPR-facilitating parallel fibers and where only the former is modulated via presynaptic α_2-noradrenergic receptors) (59). Given the complexities of dendritic filtering and integration, one could speculate that differential modulation may reflect a need of processing inputs differently according to one or multiple of these reasons: different electrotonic distance of the synapses (60), different spike timing onsets, intrinsically different activity patterns of the originating cells, or different nature of the information conveyed by the inputs. With respect to this latter aspect, lesion studies brought to propose that LPP and MPP indeed convey different information into the hippocampus (61, 62), more sensory-related the LPP, limbic state-related the MPP (61). Moreover, information about spatial location might be preferentially carried by LPP afferents, while signals related to attention, motivation, and drive might be preferentially carried by MPP ones (63). Thus, differential modulation of one but not the other pathway may reshape local dendritic computation, enabling pathway-specific long-term information storage and transfer and ultimately, different cognitive outcomes.

In line with the above considerations, pre-NMDAR–dependent modulation likely contributes to the large outcome differences in physiology of MPP vs. LPP synapses [e.g., in release probability and LTP forms (64, 65)] and in the different susceptibility to pathology (3, 4). Modified LTP at MPP-GC synapses in GluN3a$^{-/-}$ mice reveals the contribution of GluN3a-containing pre-NMDARs to the properties of synaptic plasticity of these synapses. By enhancing release probability, pre-NMDARs strengthen MPP-GC connectivity in conditions of sparse firing, but during high-frequency periods, the pre-NMDAR effect may actually reduce their dynamic range for potentiation. Thus, the enhanced LTP seen in GluN3a$^{-/-}$ mice (or on suppression of astrocyte Ca^{2+} elevations) likely reflects lack of a basal "prepotentiation" state imposed by pre-NMDARs in the normal mice. Importantly, we have recently described that inflammation causes excessive pre-NMDAR activation via astrocyte TNFR1-dependent signaling in a mouse model of multiple sclerosis. Alteration of the modulatory input in turn causes PP-GC synapses to be persistently set to a high-release probability mode, an effect that we found to be associated to impaired contextual memory (14).

Prominent and diverse impacts of GluN3a expression on NMDAR-dependent long-term synaptic plasticity have been previously reported in various circuits, notably in the hippocampus (66–68) and visual cortex (34, 43), but astrocytes were never described before as activators of such receptors. For instance, an increase in LTP on GluN3a knockout (and decrease on GluN3a overexpression) had been already reported in both the CA1 hippocampus and DG (66–68), but the effects of GluN3a were deemed to be postsynaptic, and the role of this subunit was mainly interpreted as a "brake," preventing synapse maturation and full expression of NMDAR-dependent plasticity (58, 67). In the visual cortex, GluN3a was found to be required for induction of pre-NMDAR–dependent spike-timing dependent long-term depression (t-LTD) at L4-to-L2/3 synapses, and its expression was found to be regulated in an age-dependent fashion and modulated by sensory experience in the adult life (34, 43). While no role for astrocytes was described in the activation of these GluN3a-containing pre-NMDARs, an earlier t-LTD study at barrel cortex L4-to-L2/3 synapses did in fact implicate astrocytic glutamate release as a key requirement for pre-NMDAR activation (35) but did not explore the involvement of GluN3a.

At MPP-GC synapses, transition from the developmental period into adulthood is accompanied by partially reduced expression of GluN3a subunits and of functional GluN3a-containing pre-NMDARs, akin to the observations in the visual cortex. This could identify further refinement of the circuitry with a more selected group of MPP-GC synapses undergoing GluN3a-dependent pre-NMDAR modulation but also, the shift to a different type of modulation at synapses that lose expression of GluN3a but not of other subunits, like GluN2b. Thus, GluN3a-lacking pre-NMDAR will become Mg^{2+} sensitive and require more stringent conditions for activation, like coincident depolarization of the terminals to relieve the Mg^{2+} block. This switch may, therefore, restrict circumstances in which release probability is boosted, impacting on control of LTP and in general, on computations of this synaptic circuit.

Future work will need to address the above points and some additional critical aspects raised by these findings. Why is selective modulation of the MPP input needed? What does this input carry to GC dendritic computations that is different from the LPP input and might require differential plasticity to enforce? What are the implications for the pathologies selectively affecting LPP vs. MPP, such as AD (3, 4)? Why and how are astrocytes called to participate in this control but only at one of the two pathways? What is the molecular effector system controlling synaptic release probability downstream of pre-NMDAR activation?

Materials and Methods

Brain Slices. Mice were deeply anesthetized with isoflurane and decapitated in accordance with the authorizations concerning animal experimentation procedures of the Veterinary Office of the Canton de Vaud (Switzerland). Horizontal hippocampal slices (350-μm thick) for electrophysiology experiments were prepared from P17 to P22 mice, except for LTP (P17–P30) and age-related (P20–P40) experiments, using a vibrating blade microtome (HM 650 V Microm or Leica VT1000). The cold slicing solution contained (in millimolar) 62.5 NaCl, 2.5 KCl, 7 $MgCl_2$, 0.5 $CaCl_2$, 25 $NaHCO_3$, 1.5 NaH_2PO_4, 10 glucose, and 105 sucrose at pH 7.4 (bubbled with a mixture of 95% O_2 and 5% CO_2). After cutting, slices were kept in aCSF in a submersion chamber at 34 °C for 5–6 h. aCSF used for electrophysiology recordings contained (in millimolar) 125 NaCl, 2 KCl, 2 $MgCl_2$, 2 $CaCl_2$ (except for a set of experiments in low Ca^{2+}, in which only 1 $CaCl_2$ was present), 25 $NaHCO_3$, 1.2 NaH_2PO_4, and 10 glucose at nominal pH 7.4 (bubbled with a mixture of 95% O_2 and 5% CO_2).

Electrophysiology. All recordings were performed at 34 °C. Inhibitory γ-aminobutyric acid receptor type A-mediated currents and action potentials were routinely blocked unless otherwise indicated by adding picrotoxin (100 μM) and TTX (1 μM), respectively, to the recording solution. In specific sets of experiments, NMDAR-mediated currents were blocked by adding D-APV (50 μM), ifenprodil (3 μM), or 7-chlorokynurenic acid (100 μM) as indicated. Hippocampal DG GCs were visually identified under infrared differential interference contrast mode using an infrared camera and an upright fixed-stage microscope (Olympus BX51WI). In many experiments, whole-cell recordings from GCs were made with ∼3- to 5-MΩ patch pipettes containing (in millimolar) 117.5 Cs gluconate, 17.5 CsCl, 10 4-(2-hydroxyethyl)-1-piperazineethanesulfonic acid (Hepes), 0.2 ethylene glycol-bis(β-aminoethyl ether)-*N,N,N′,N′*-tetraacetic acid, 8 NaCl, 2 MgATP, 0.3 NaGTP, 5 QX314, and 1 MK-801 (pH 7.2, osmolarity: 295 mOsm). AMPAR-mediated mEPSCs were recorded from GCs kept at −80 mV holding potential in the presence of intracellular MK-801 (1 mM) and 2 mM extracellular Mg^{2+} to minimize activation of postsynaptic NMDARs (10). Combining GC hyperpolarization to intracellular MK-801 was useful toward this end, as intracellular MK-801 was recently reported to not always block NMDAR completely (69). Patched cells were kept for at least 15 min before NMDA puff to allow MK801 to diffuse to distal dendrites. The gap-free traces were acquired using the MultiClamp 700B amplifier and digitized at 50 kHz using Digidata 1440. Synaptic currents were low-pass filtered at 1 kHz using a four-pole Bessel filter. In other sets of experiments, electrically evoked synaptic currents, either eEPSCs or fEPSPs, were measured. Electrical stimulations were selectively targeted toward MPP or LPP inputs by placing the stimulating electrode in the middle or outer one-third of the dentate molecular layer, respectively. For paired pulse measurements, the two pulses were separated by 50 ms (20 Hz), and each test pulse was delivered once every 20 or 30 s. In some experiments, we utilized a 30-Hz stimulation protocol to deplete the RRP of synaptic vesicles (54). For experiments assessing LTP, electrodes for field measurement were inserted into the middle one-third of the molecular layer. The LTP induction protocol consisted of two to three HFSs of 100 pulses for 1 s each separated by an interval of 20 s; experiments were performed in 2 mM Mg^{2+} and without addition of any antagonists. To probe the role of astrocytic Ca^{2+} signaling in LTP, we patched an astrocyte located proximally to the field electrode, and dialyzed it with the Ca^{2+} chelator BAPTA (40 mM) (10, 13, 15).

For field recordings, stimulation strength was chosen to correspond approximately to 30–40% of the maximal response. Input–output curves were measured by gradually incrementing the stimulation strength by 10 μA per sweep (delivered every 30 s). The data were discarded if the series resistance changed over 20% (for whole-cell experiments) or if the fEPSP amplitude changed over 15% in 15 min before the stimulation (for field recording experiments).

GluN3a Knockout Mice. GluN3a $^{-/-}$ mice (also known as NR3a $^{-/-}$) were generated as previously reported (51) and maintained as heterozygotes. They developed normally and were not perceptibly different from littermate controls by body weight or apparent behavior, despite that some differences were previously reported (66). Electrophysiological investigations were performed in homozygous GluN3a ($^{-/-}$) and wild-type controls (age: P17–P22). For the latter, we used both GluN3a$^{+/+}$ littermates and B6 wild-type mice, and since no differences were found between the two groups, we pooled them together. After performing electrophysiological experiments, the exact genotype of each tested mouse was determined by RT-PCR analysis of the tails as described previously (51, 70). Mice of both genders were used.

NMDA Local Puff Application. Local puff application of aCSF or NMDA at various concentrations (0.5–5 μM) was performed using an electronically controlled picospritzer (PV830 pneumatic PicoPump) as previously described (14). The ejection pipette was positioned in the dentate molecular layer, and a single 10-s pulse (4–7 psi) was applied. Spatial diffusion was indirectly verified in some experiments by coejecting a fluorescent dye under two-photon imaging. At plateau, diffusion of the dye invested a spherical volume with ∼25-μm radius. Local administration avoids indirect NMDA-dependent effects on PP axons mediated by activation of somatodendritic receptors on distal pyramidal cells in EC.

Analysis. Continuous current traces recorded from GCs were split into 60-s episodes and mEPSC events detected using Mini analysis software (v6.0, Synaptosoft) under continuous user supervision. From these data, average event frequency, amplitude, and kinetics (rise and decay time constants) were automatically calculated for each experimental time point (a single 60-s stretch). Percentage increase after NMDA application was calculated by dividing mEPSC frequency observed after NMDA puff by baseline frequency recorded 1 min before NMDA puff. Based on initial time course experiments examining the NMDA effect between 1 and 30 min from puff application and previous observations of pre-NMDAR–dependent mEPSC modulation by tumor necrosis factor-α (14), the 20-min time was chosen as plateau of the drug effects. Amplitudes and PPRs of the evoked currents were measured in Clampfit. PPR was calculated as the amplitude of peak 2 divided by the amplitude of peak 1.

Statistics. Statistical significance of the observations was evaluated using unpaired Student's *t* (two sided), ANOVA, χ^2, and Kolmogorov–Smirnov (KS) tests as indicated. The cumulative distributions were compared using nonparametric KS test. Nonparametric Kruskal–Wallis tests with multiple comparisons procedure were performed using Dataplot (NIST). For *t* tests, normality was tested using Shapiro–Wilk (Origin 8 software; OriginLab). For Fig. 4*B*, both one-way and two-way ANOVAs were performed. Results for the one-way ANOVA are reported in Fig. 4*B*, and Levene's test indicates that population variances are significantly different at the 0.05 level. Results for the two-way ANOVA are as follows: statistically significant difference was found (at $P < 0.05$) for age and synaptic input (MPP vs. LPP) factors (Tukey means comparison). All results are reported as averages ± SEM unless otherwise indicated. Each experiment has been replicated multiple times (at least three different mice). Sample sizes were chosen based on the values sufficient to observe statistical significance in the prior studies. Randomization was not used.

Immunohistochemistry for EM. Immunohistochemical reactions for EM were carried out using the preembedding immunogold method described previously (71). Briefly, free-floating sections were incubated in 10% (vol/vol) normal goat serum (NGS) diluted in Tris-buffered saline (TBS). Sections were then incubated in an anti-GluN3a antibody [3–5 μg/mL diluted in TBS containing 1% (vol/vol) NGS]. Antibody specificity was previously confirmed by experiments in GluN3a knockout mice (72). This was followed by incubation in goat anti-mouse immunoglobulin G coupled to 1.4-nm gold (Nanoprobes Inc.). Sections were postfixed in 1% (vol/vol) glutaraldehyde and washed in double-distilled water followed by silver enhancement of the gold particles with an HQ Silver kit (Nanoprobes Inc.). Sections were then treated with osmium tetraoxide (1% in 0.1 M phosphate buffer), block stained with uranyl acetate, dehydrated in graded series of ethanol, and flat embedded on glass slides in Durcupan (Fluka) resin. Regions of interest were cut at 70–90 nm on an ultramicrotome (Reichert Ultracut E; Leica) and collected on single-slot pioloform-coated copper grids. Staining was performed on drops of 1% aqueous uranyl acetate followed by Reynolds's lead citrate. Ultrastructural analyses were performed in a Jeol-1010 electron microscope.

Quantification of GluN3a Immunoreactivity. To establish the relative abundance of GluN3a immunoreactivity in the MPP or LPP of the DG molecular layer, 60-μm-thick coronal slices were processed for preembedding immunogold immunohistochemistry (see above). Embedding blocks were prepared using three samples of tissue per mouse from three mice at either P21 or P45 (totaling nine blocks per age). To minimize false negatives, electron microscopic serial ultrathin sections were cut close to the surface of each block, as immunoreactivity decreased with depth. We estimated the quality of immunolabeling by always selecting areas with optimal gold labeling at approximately the same distance from the cutting surface. Randomly selected areas were then photographed from the selected ultrathin sections and printed with a final magnification of 60,000×. We counted immunoparticles identified in each reference area and present along the plasma membrane in two different subcellular compartments: dendritic spines and axon terminals. Profiles were selected for sampling when dendritic spines or axon terminals contained at least one gold particle.

Data Availability. All data necessary to evaluate the conclusions of the paper are contained in the figures. The original recordings are stored on the institutional server and are available from the corresponding author on reasonable request.

ACKNOWLEDGMENTS. This work was supported by European Research Council Grant Advanced, 340368 "Astromnesis"; Swiss National Science Foundation Grants 31003A-173124/1, 51NF40-160620 [National Center of Competence in Research (NCCR) "Transcure"], and 51NF40-158776 (NCCR "Synapsy"); Synapsis Foundation Grant 2018-PI01 (to A.V.); Spanish Ministry of Education and Science Grant BFU2015-63769-R; and Junta de Comunidades de Castilla-La Mancha Grant PPII-2014-005-P (to R.L.). We thank Claire Cooper and Nicolas Liaudet for participating in pilot experiments and analyses. We also thank Nobuki Nakanishi and Stuart Lipton for providing GluN3a$^{-/-}$ mice and Isabel Perez-Otano for helpful discussions and advice.

1. N. Burgess, E. A. Maguire, J. O'Keefe, The human hippocampus and spatial and episodic memory. *Neuron* **35**, 625–641 (2002).
2. D. Paré, M. deCurtis, R. Llinás, Role of the hippocampal-entorhinal loop in temporal lobe epilepsy: Extra- and intracellular study in the isolated Guinea pig brain in vitro. *J. Neurosci.* **12**, 1867–1881 (1992).
3. G. W. Van Hoesen, B. T. Hyman, A. R. Damasio, Entorhinal cortex pathology in Alzheimer's disease. *Hippocampus* **1**, 1–8 (1991).
4. M. Llorens-Martín *et al*., Selective alterations of neurons and circuits related to early memory loss in Alzheimer's disease. *Front. Neuroanat.* **8**, 38 (2014).
5. M. Y. Min, F. Asztely, M. Kokaia, D. M. Kullmann, Long-term potentiation and dual-component quantal signaling in the dentate gyrus. *Proc. Natl. Acad. Sci. U.S.A.* **95**, 4702–4707 (1998).
6. A. Scimemi, S. Schorge, D. M. Kullmann, M. C. Walker, Epileptogenesis is associated with enhanced glutamatergic transmission in the perforant path. *J. Neurophysiol.* **95**, 1213–1220 (2006).
7. J. F. Reilly *et al*., Amyloid deposition in the hippocampus and entorhinal cortex: Quantitative analysis of a transgenic mouse model. *Proc. Natl. Acad. Sci. U.S.A.* **100**, 4837–4842 (2003).
8. U. A. Khan *et al*., Molecular drivers and cortical spread of lateral entorhinal cortex dysfunction in preclinical Alzheimer's disease. *Nat. Neurosci.* **17**, 304–311 (2014).
9. D. J. Froc *et al*., Reduced synaptic plasticity in the lateral perforant path input to the dentate gyrus of aged C57BL/6 mice. *J. Neurophysiol.* **90**, 32–38 (2003).
10. P. Jourdain *et al*., Glutamate exocytosis from astrocytes controls synaptic strength. *Nat. Neurosci.* **10**, 331–339 (2007).
11. P. Bezzi *et al*., Astrocytes contain a vesicular compartment that is competent for regulated exocytosis of glutamate. *Nat. Neurosci.* **7**, 613–620 (2004).
12. M. K. Schwarz *et al*., Fluorescent-protein stabilization and high-resolution imaging of cleared, intact mouse brains. *PLoS One* **10**, e0124650 (2015).
13. M. Santello, P. Bezzi, A. Volterra, TNFα controls glutamatergic gliotransmission in the hippocampal dentate gyrus. *Neuron* **69**, 988–1001 (2011).
14. S. Habbas *et al*., Neuroinflammatory TNFα impairs memory via astrocyte signaling. *Cell* **163**, 1730–1741 (2015).
15. M. A. Di Castro *et al*., Local Ca2+ detection and modulation of synaptic release by astrocytes. *Nat. Neurosci.* **14**, 1276–1284 (2011).
16. P. Paoletti, C. Bellone, Q. Zhou, NMDA receptor subunit diversity: Impact on receptor properties, synaptic plasticity and disease. *Nat. Rev. Neurosci.* **14**, 383–400 (2013).
17. C. G. Lau, R. S. Zukin, NMDA receptor trafficking in synaptic plasticity and neuropsychiatric disorders. *Nat. Rev. Neurosci.* **8**, 413–426 (2007).
18. E. B. Bloss *et al*., Single excitatory axons form clustered synapses onto CA1 pyramidal cell dendrites. *Nat. Neurosci.* **21**, 353–363 (2018).
19. N. Toni *et al*., Synapse formation on neurons born in the adult hippocampus. *Nat. Neurosci.* **10**, 727–734 (2007).
20. N. O. Dalby, I. Mody, Activation of NMDA receptors in rat dentate gyrus granule cells by spontaneous and evoked transmitter release. *J. Neurophysiol.* **90**, 786–797 (2003).
21. M. Casado, S. Dieudonné, P. Ascher, Presynaptic N-methyl-D-aspartate receptors at the parallel fiber-Purkinje cell synapse. *Proc. Natl. Acad. Sci. U.S.A.* **97**, 11593–11597 (2000).
22. D. J. Brasier, D. E. Feldman, Synapse-specific expression of functional presynaptic NMDA receptors in rat somatosensory cortex. *J. Neurosci.* **28**, 2199–2211 (2008).
23. P. J. Sjöström, G. G. Turrigiano, S. B. Nelson, Neocortical LTD via coincident activation of presynaptic NMDA and cannabinoid receptors. *Neuron* **39**, 641–654 (2003).
24. A. Rodríguez-Moreno, O. Paulsen, Spike timing-dependent long-term depression requires presynaptic NMDA receptors. *Nat. Neurosci.* **11**, 744–745 (2008).
25. C. Bidoret, A. Ayon, B. Barbour, M. Casado, Presynaptic NR2A-containing NMDA receptors implement a high-pass filter synaptic plasticity rule. *Proc. Natl. Acad. Sci. U.S.A.* **106**, 14126–14131 (2009).
26. A. Rodríguez-Moreno *et al*., Presynaptic self-depression at developing neocortical synapses. *Neuron* **77**, 35–42 (2013).
27. H. Park, A. Popescu, M. M. Poo, Essential role of presynaptic NMDA receptors in activity-dependent BDNF secretion and corticostriatal LTP. *Neuron* **84**, 1009–1022 (2014).
28. M. Pérez-Rodríguez *et al*., Adenosine receptor-mediated developmental loss of spike timing-dependent depression in the hippocampus. *Cereb. Cortex* 10.1093/cercor/bhy194 (2018).
29. B. Rossi *et al*., Current and calcium responses to local activation of axonal NMDA receptors in developing cerebellar molecular layer interneurons. *PLoS One* **7**, e39983 (2012).
30. K. Dore *et al*., Unconventional NMDA receptor signaling. *J. Neurosci.* **37**, 10800–10807 (2017).
31. P. M. Lachamp, Y. Liu, S. J. Liu, Glutamatergic modulation of cerebellar interneuron activity is mediated by an enhancement of GABA release and requires protein kinase A/RIM1alpha signaling. *J. Neurosci.* **29**, 381–392 (2009).
32. I. C. Duguid, T. G. Smart, Retrograde activation of presynaptic NMDA receptors enhances GABA release at cerebellar interneuron-Purkinje cell synapses. *Nat. Neurosci.* **7**, 525–533 (2004).
33. A. Rodríguez-Moreno *et al*., Presynaptic induction and expression of timing-dependent long-term depression demonstrated by compartment-specific photorelease of a use-dependent NMDA receptor antagonist. *J. Neurosci.* **31**, 8564–8569 (2011).
34. R. S. Larsen *et al*., NR3A-containing NMDARs promote neurotransmitter release and spike timing-dependent plasticity. *Nat. Neurosci.* **14**, 338–344 (2011).
35. R. Min, T. Nevian, Astrocyte signaling controls spike timing-dependent depression at neocortical synapses. *Nat. Neurosci.* **15**, 746–753 (2012).
36. B. C. Carter, C. E. Jahr, Postsynaptic, not presynaptic NMDA receptors are required for spike-timing-dependent LTD induction. *Nat. Neurosci.* **19**, 1218–1224 (2016).
37. J. R. Pugh, C. E. Jahr, NMDA receptor agonists fail to alter release from cerebellar basket cells. *J. Neurosci.* **31**, 16550–16555 (2011).
38. G. Bouvier, R. S. Larsen, A. Rodríguez-Moreno, O. Paulsen, P. J. Sjöström, Towards resolving the presynaptic NMDA receptor debate. *Curr. Opin. Neurobiol.* **51**, 1–7 (2018).
39. R. Corlew, Y. Wang, H. Ghermazien, A. Erisir, B. D. Philpot, Developmental switch in the contribution of presynaptic and postsynaptic NMDA receptors to long-term depression. *J. Neurosci.* **27**, 9835–9845 (2007).
40. A. Banerjee *et al*., Double dissociation of spike timing-dependent potentiation and depression by subunit-preferring NMDA receptor antagonists in mouse barrel cortex. *Cereb. Cortex* **19**, 2959–2969 (2009).
41. Y. Andrade-Talavera, P. Duque-Feria, O. Paulsen, A. Rodríguez-Moreno, Presynaptic spike timing-dependent long-term depression in the mouse hippocampus. *Cereb. Cortex* **26**, 3637–3654 (2016).
42. K. A. Buchanan *et al*., Target-specific expression of presynaptic NMDA receptors in neocortical microcircuits. *Neuron* **75**, 451–466 (2012).
43. R. S. Larsen *et al*., Synapse-specific control of experience-dependent plasticity by presynaptic NMDA receptors. *Neuron* **83**, 879–893 (2014).
44. S. F. Traynelis *et al*., Glutamate receptor ion channels: Structure, regulation, and function. *Pharmacol. Rev.* **62**, 405–496 (2010).
45. J. Prius-Mengual, M. Pérez-Rodríguez, Y. Andrade-Talavera, A. Rodríguez-Moreno, NMDA receptors containing GluN2B/2C/2D subunits mediate an increase in glutamate release at hippocampal CA3-CA1 synapses. *Mol. Neurobiol.* **56**, 1694–1706 (2019).
46. S. Pachernegg, N. Strutz-Seebohm, M. Hollmann, GluN3 subunit-containing NMDA receptors: Not just one-trick ponies. *Trends Neurosci.* **35**, 240–249 (2012).
47. J. E. Chatterton *et al*., Excitatory glycine receptors containing the NR3 family of NMDA receptor subunits. *Nature* **415**, 793–798 (2002).
48. C. T. Smothers, J. J. Woodward, Pharmacological characterization of glycine-activated currents in HEK 293 cells expressing N-methyl-D-aspartate NR1 and NR3 subunits. *J. Pharmacol. Exp. Ther.* **322**, 739–748 (2007).
49. S. Nabavi *et al*., Metabotropic NMDA receptor function is required for NMDA receptor-dependent long-term depression. *Proc. Natl. Acad. Sci. U.S.A.* **110**, 4027–4032 (2013).
50. J. Aow, K. Dore, R. Malinow, Conformational signaling required for synaptic plasticity by the NMDA receptor complex. *Proc. Natl. Acad. Sci. U.S.A.* **112**, 14711–14716 (2015).
51. S. Das *et al*., Increased NMDA current and spine density in mice lacking the NMDA receptor subunit NR3A. *Nature* **393**, 377–381 (1998).
52. L. A. Kehoe *et al*., GluN3A promotes dendritic spine pruning and destabilization during postnatal development. *J. Neurosci.* **34**, 9213–9221 (2014).
53. N. Berretta, R. S. Jones, Tonic facilitation of glutamate release by presynaptic N-methyl-D-aspartate autoreceptors in the entorhinal cortex. *Neuroscience* **75**, 339–344 (1996).
54. T. Abrahamsson *et al*., Differential regulation of evoked and spontaneous release by presynaptic NMDA receptors. *Neuron* **96**, 839–855.e5 (2017).
55. C. Henneberger, T. Papouin, S. H. Oliet, D. A. Rusakov, Long-term potentiation depends on release of D-serine from astrocytes. *Nature* **463**, 232–236 (2010).
56. E. Bindocci *et al*., Three-dimensional Ca^{2+} imaging advances understanding of astrocyte biology. *Science* **356**, eaai8185 (2017).
57. K. B. Hansen *et al*., Structure, function, and allosteric modulation of NMDA receptors. *J. Gen. Physiol.* **150**, 1081–1105 (2018).
58. I. Pérez-Otaño, R. S. Larsen, J. F. Wesseling, Emerging roles of GluN3-containing NMDA receptors in the CNS. *Nat. Rev. Neurosci.* **17**, 623–635 (2016).
59. M. R. Carey, W. G. Regehr, Noradrenergic control of associative synaptic plasticity by selective modulation of instructive signals. *Neuron* **62**, 112–122 (2009).
60. F. W. Grillo *et al*., A distance-dependent distribution of presynaptic boutons tunes frequency-dependent dendritic integration. *Neuron* **99**, 275–282.e3 (2018).
61. J. Ferbinteanu, R. M. Holsinger, R. J. McDonald, Lesions of the medial or lateral perforant path have different effects on hippocampal contributions to place learning and on fear conditioning to context. *Behav. Brain Res.* **101**, 65–84 (1999).
62. T. Myhrer, The role of medial and lateral hippocampal perforant path lesions and object distinctiveness in rats' reaction to novelty. *Physiol. Behav.* **42**, 371–377 (1988).
63. M. P. Witter, T. P. Doan, B. Jacobsen, E. S. Nilssen, S. Ohara, Architecture of the entorhinal cortex a review of entorhinal anatomy in rodents with some comparative notes. *Front. Syst. Neurosci.* **11**, 46 (2017).
64. C. R. Bramham, K. Bacher-Svendsen, J. M. Sarvey, LTP in the lateral perforant path is beta-adrenergic receptor-dependent. *Neuroreport* **8**, 719–724 (1997).

65. M. R. Hunsaker, G. G. Mooy, J. S. Swift, R. P. Kesner, Dissociations of the medial and lateral perforant path projections into dorsal DG, CA3, and CA1 for spatial and non-spatial (visual object) information processing. *Behav. Neurosci.* **121**, 742–750 (2007).
66. O. Mohamad, M. Song, L. Wei, S. P. Yu, Regulatory roles of the NMDA receptor GluN3A subunit in locomotion, pain perception and cognitive functions in adult mice. *J. Physiol.* **591**, 149–168 (2013).
67. A. C. Roberts *et al*., Downregulation of NR3A-containing NMDARs is required for synapse maturation and memory consolidation. *Neuron* **63**, 342–356 (2009).
68. M. L. Brady *et al*., Moderate prenatal alcohol exposure reduces plasticity and alters NMDA receptor subunit composition in the dentate gyrus. *J. Neurosci.* **33**, 1062–1067 (2013).
69. W. Sun, J. M. Wong, J. A. Gray, B. C. Carter, Incomplete block of NMDA receptors by intracellular MK-801. *Neuropharmacology* **143**, 122–129 (2018).
70. N. J. Sucher *et al*., Developmental and regional expression pattern of a novel NMDA receptor-like subunit (NMDAR-L) in the rodent brain. *J. Neurosci.* **15**, 6509–6520 (1995).
71. R. Lujan, Z. Nusser, J. D. Roberts, R. Shigemoto, P. Somogyi, Perisynaptic location of metabotropic glutamate receptors mGluR1 and mGluR5 on dendrites and dendritic spines in the rat hippocampus. *Eur. J. Neurosci.* **8**, 1488–1500 (1996).
72. I. Pérez-Otaño *et al*., Endocytosis and synaptic removal of NR3A-containing NMDA receptors by PACSIN1/syndapin1. *Nat. Neurosci.* **9**, 611–621 (2006).